Biochimica et Biophysica Acta 1840 (2014) 1092–1104

Contents lists available at ScienceDirect

Biochimica et Biophysica Acta

journal homepage: www.elsevier.com/locate/bbagen

Metabolomics and transcriptomics demonstrate severe oxidative stress in both localized chemotherapy-treated and bystander tumors

Daniel Morvan [a,b,1], Aicha Demidem [c,*,1]

[a] UDA University, 49 Boulevard François Mitterrand, CS 60032, 63001 Clermont Ferrand Cedex 1, France
[b] Centre Jean Perrin, 58 Rue Montalembert, F-63011 Clermont Ferrand, France
[c] UMR 1019 INRA/UDA University, ECREIN, Laboratoire de Biochimie Biologie Moléculaire, Faculté de Pharmacie, 28 Place Henri Dunant, F-63001 Clermont Ferrand, France

ARTICLE INFO

Article history:
Received 16 July 2013
Received in revised form 4 November 2013
Accepted 22 November 2013
Available online 1 December 2013

Keywords:
Chemotherapy
Bystander tumor
Metabolomics
Transcriptomics
Oxidative stress

ABSTRACT

Background: Localized radiotherapy is long known to cause damages to not only targeted but also non-targeted cells, the so-called bystander (BS) effect. Recently, BS effect was demonstrated in response to chemotherapy. To get further insight into the mechanism of chemotherapy-induced BS effect in vivo, we investigated the response of normal tissues and untreated BS melanomas, at distance from localized chemotherapy-treated melanomas.
Methods: B16 melanoma cells were inoculated *sc* in one flank, in mice. Chemotherapy was administered intratumorally. After 3 weeks, untreated melanomas were implanted into the other flank. Tumors were analyzed morphologically, and using metabolomics and transcriptomics.
Results: Locally-treated melanomas showed growth inhibition and pleiotropic metabolic and transcriptional alterations. Tumors recovered slow proliferation while exhibiting prominent oxidative stress response (decreased glutathione level, and increased expression of genes including Mt1, Gpx3, Sod3, and Hmox1). Plasma contained increased levels of oxidative stress products. However, liver and soleus muscle displayed unaltered morphological characteristics. In contrast, untreated BS melanomas induced from naive B16 cells showed reduced growth, marked oxidative stress response (decreased glutathione level, and increased expression of genes including Sod2, Gpx1 and Gsr), and ras oncogene expression alterations. Furthermore, metabolomics and transcriptomics enabled to estimate the proportion of cells undergoing the BS effect within treated tumors.
Conclusion: Treatment of tumors with chemotherapy induces BS effects, underpinned by oxidative stress, in abnormal proliferating tissues in vivo, not in normal tissue, that significantly contribute to overall tumor response. General significance BS effect significantly contributes to response to chemotherapy, and may be exploited to improve overall response to cancer treatment.

1. Introduction

A longstanding paradigm has been that radiation hits to the cell nucleus was required for genetic damage and biological responses. During the last decades, this view has been challenged by the demonstration of radiation-induced effects in non irradiated cells neighboring or cocultured with radiation-targeted cells, the so-called radiation-induced bystander (BS) effect [1–3].

Several lines of evidence have implicated radiotherapy-induced BS effet in in vivo responses, including DNA damage in normal tissue at distance from localized radiotherapy [4], and oncogenesis in mice genetically predisposed to cerebellar tumors at distance from the radiotherapy area [5,6]. In addition, clinically, abscopal responses to radiotherapy have been attributed to the BS effect [7,8]. Although less documented, we and others have reported that BS effect may occur in response to chemotherapy, in vitro and in vivo [9–12].

A major feature of cells undergoing radiotherapy- or chemotherapy-induced BS effect is genomic instability and DNA damage [11,13]. In addition, a body of evidence implicates oxidative metabolism and gap-junction intercellular communication in the transmission of signal from directly targeted to BS cells not only in vitro, but also in vivo [5,6]. Other mechanisms involving cyclooxygenase 2, the protein kinase-C family, and ATM/ATR have been proposed to play a role in signaling BS effect [14]. Actin skeleton, Rho kinase and reactive oxygen species (ROS) were implicated in chemotherapy-induced BS effect in vitro and in vivo [10,11]. Several soluble factors, candidates to the BS mediator, have been proposed, including TGFβ, NO and ATP [15,16]. Among them, ATP was recently shown to be released by chemotherapy-treated cells, and participate to immunogenic elimination of tumor cells [17,18], a putative mechanism for BS effect.

Abbreviations: BS, bystander; *i.p.*, intraperitoneal; *i.t.*, intratumor; CTL, control; INH, inhibition phase; REC, recovery phase

* Corresponding author at: Laboratoire de Biochimie Biologie Moléculaire, Faculty of Pharmacy, 28 Place Henri Dunant, F-63001 Clermont Ferrand, France. Tel.: +33 4 731 78047.
E-mail addresses: ademidem@clermont.inra.fr (D. Morvan), Daniel.Morvan@udamail.fr (A. Demidem).

[1] Contributed equally to this study.

0304-4165/$ – see front matter © 2013 Elsevier B.V. All rights reserved.
http://dx.doi.org/10.1016/j.bbagen.2013.11.022

To get further insight into the mechanism of chemotherapy-induced BS effect in vivo, the response of distant normal tissues and BS melanomas obtained after re-inoculation of naïve B16 cells was compared with that of melanomas treated by localized chemotherapy consisting in intratumor (*i.t.*) administration of fotemustine, a classical treatment for melanoma. Treatment by *i.t.* administration was performed to preserve as much as possible immunocompetence of mice, and spatially confine direct chemotherapy effects to the treated tumor.

Instead of evaluating BS effect from features of genomic instability, which we previously demonstrated in chemotherapy-induced BS effect in vitro and in vivo [10], we performed molecular screening of metabolic and transcriptional alterations in tumors, an approach devoid of preconception and increasingly used to get a comprehensive view of phenotype changes. Fotemustine-treated melanomas underwent growth arrest and displayed pleiotropic central metabolism and transcriptional alterations, including commutation from glycolysis to Krebs cycle, oxidative stress response and oncogenic alterations. Then, treated melanomas recovered reduced proliferation, but displayed still pronounced oxidative stress response, and other alterations involving lipid metabolism, DNA repair, and cell signaling. Meanwhile, liver and soleus muscle showed unaltered morphological characteristics. In contrast, untreated BS melanomas induced from naive B16 cells showed reduced growth, pronounced oxidative stress response, and ras proto-oncogene expression changes, prominently implicating mitochondria. Multivariate statistical analysis of metabolic and transcriptional data enabled to estimate the within-treated tumor BS effect to about 45%. In addition, over the long term, the plasma of mice harboring a fotemustine-treated tumor was shown to contain increased levels of oxidative stress markers.

In conclusion, localized chemotherapy appears to not injure distant normal tissue but induces severe oxidative stress response in untreated BS tumors. This study also proposes an approach to evaluate the contribution of BS effect within localized therapy-treated tumors. It identifies BS effect as a significantly contributing response to chemotherapy that may be exploited to improve overall response to cancer treatment.

2. Materials and methods

2.1. Chemicals

A chloroethylnitrosourea, fotemustine (N′-(2-chloroethyl)-N-(2-(methylsulphonyl)-ethyl)-N′-nitrosourea), was used in experiments, and dissolved (5 mM) in 0.9% NaCl before use. DL-[1,2-^{13}C]glucose (99% ^{13}C-nucleus enriched, tested for biological purity) was purchased from Eurisotop, Gif-sur-Yvette, France. Water-d2 (Peypin, France) was used for locking the NMR spectrometer.

2.2. Cell culture

The transplantable B16 (F1) melanoma cells originating from C57BL6/6J Ico mice were obtained from ICIG (Villejuif, France), and adapted to grow in culture. Melanocytes were maintained as monolayers in culture flasks using culture medium consisting of Eagle's MEM-glutaMAX medium (Life technologies). Cells were harvested by trypsinization, washed into PBS, centrifuged, and kept at −80 °C until inoculation.

2.3. Animal care

The experiment was carried out with C57BL6/6J male mice aged 6–7 weeks weighing about 20–22 g, obtained from IFFA CREDO, France. Mice were housed by 3 in a polypropylene cage. They were provided with free access to standard diet and water. The animals were maintained in a controlled environment under standard conditions of temperature and humidity, with an alternating 12 h light/dark cycle, in accordance with the guidelines of the Animal Experimental Ethical Committee from INSERM. Mice were monitored at least every 2 day for welfare including weight, physical appearance, behavior and measurable clinical signs. The study protocol was approved by the Animal Experimental Ethical Committee from INSERM, France.

2.4. Experimental protocols

C57BL6/6J recipients were inoculated with 5×10^5 syngeneic B16 melanoma cells in 100 μl physiological serum in one flank at day 1. The B16 F1 cell line used in experiments was not metastatic. In a first experiment (Fig. 1A), mice were assigned to 3 recipient groups, a recipient group bearing an untreated tumor (control, CTL, n = 7), and 2 recipient groups with a tumor treated with fotemustine intratumorally (*i.t.*). Fotemustine was administered at a dose of 15 μg/g in 150 μl physiological serum at days 11–14–18. Mice were followed for 11 days after treatment (INH, n = 11) and for 39 days after treatment (REC, n = 11). They were monitored every 2 day including body weight, physical appearance, behavior and tumor size. Tumor size was measured using calipers, and tumor mass was obtained using a classical formula [9]. During monitoring, animals were placed in an induction chamber, and reduced anesthesia with 1.5–2% isoflurane was performed. Animals sedated for 1–2 min, and were maintained warm during anesthesia.

Mice were sacrificed with humane euthanasia according to institutional guidelines for animal's welfare using the method of gas anesthesia using isoflurane >3% in oxygen. Sacrifice was performed before tumor burden reached 10% of animal body weight (or one tumor diameter reaching 20 mm) to avoid animal suffering. For the CTL group, sacrifice was performed between days 15 and 20 (Fig. 1A). For the INH group, sacrifice was performed at days 15, 20, 24 and 29, and for the REC group, at days 45, 49, 52 and 57 (Fig. 1B). Tumors and normal tissues (liver, right soleus muscle and sera) were collected from the 3 recipient groups, and prepared for analyses.

In a second experiment (Fig. 1B), mice bearing treated tumors on one flank (n = 10) were re-inoculated at day 32 with 5×10^5 parental melanoma cells in 100 μl of physiological serum *sc*, in the opposite flank, to induce a BS tumor (BS, n = 10). BS tumors were collected between days 45 and 57, before tumor burden (treated and BS tumors) reached 10% the animal body weight. At day 32, a group of mice (n = 5) was inoculated with parental B16 cells in one flank as a control group for tumor masses only (not shown in Fig. 1B). The control group undergoing analyses in this experiment was the same as that in the first experiment.

2.5. Serum transfer experiments

Total mixed blood (arterial and venous) was collected from donors bearing an untreated tumor (CTL group from the first experiment) and donors bearing a fotemustine-treated tumor (INH group) (Fig. 1C). Sera were sampled after centrifugation, and kept frozen until used. Fifty μl of each serum was administered *i.t.* to melanoma-hosting recipients at days 11, 12 and 13 from cell inoculation (n = 7 mice for each type of serum) as previously described [10]. After animal sacrifice, between days 45 and 57, tumors were removed and analyzed.

2.6. Histology

Tumor pieces were fixed in formol solution. Paraffin-embedded sections were cut into 4 μm sections, and prepared for hematoxylin–eosin staining and routine pathological analysis. Semi-quantitative histological analysis was performed. The count of mitoses was performed after hematoxylin–eosin staining on 10 microscopy fields, and quantification of anisocytosis, necrosis, pigmentation, vascularization and lymphocyte infiltration was done as follows: 0 for absent, 1 for weak, 2 for moderate, 3 for intense and 4 for very intense.

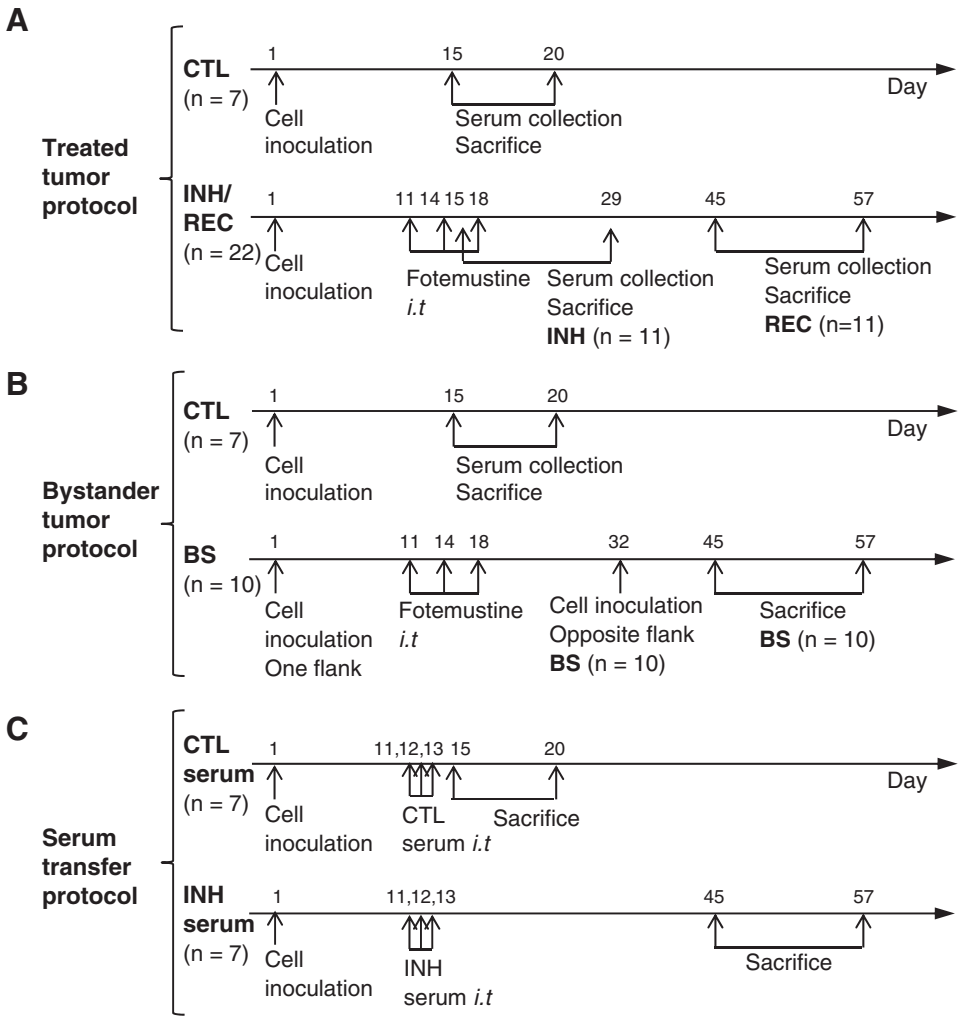

Fig. 1. Experimental protocol schema. A. Treated tumor protocol. C57BL6/6J recipients were inoculated *s.c.* with B16 melanoma cells in one flank, at day 1. Three groups of mice were performed, a group bearing an untreated tumor (CTL, n = 7) and 2 groups bearing a tumor treated *i.t.* with fotemustine at days 11–14–18 (INH, n = 11 and REC, n = 11). Mice were sacrificed between days 15–20 (CTL), days 15–29 (INH) and days 45–57 (REC). B. Bystander tumor protocol. A new REC group was obtained, then re-inoculated with B16 parental melanoma cells in the opposite flank at day 32 (BS, n = 10). Tumors were collected between days 45 and 57. The CTL group in this protocol was the same as in the treated tumor protocol. C. Serum transfer protocol. Sera from tumor-bearing untreated (CTL) and fotemustine-treated (INH) donors were taken at day 20 (CTL) or day 29 (INH) of tumor evolution. Fifty μl of each serum was administered *i.t* to melanoma tumor-hosting recipients at days 11, 12 and 13 from cell inoculation (n = 7 mice for each type of serum).

2.7. Enzyme activities

2.7.1. Pyruvate kinase (PK) activity

An aliquot of total cell protein extracts was incubated in 50 mmol l^{-1} Tris–HCl pH 7.4, 100 mmol l^{-1} KCl, 5 mmol l^{-1} $MgCl_2$, 0.6 mmol l^{-1} ADP, 0.9 mmol l^{-1} phosphoenolpyruvate, 0.3 mmol l^{-1} NADH and 2.5 IU L-lactate dehydrogenase. PK activity was measured by recording NADH oxidation at 340 nm and was calculated with one unit of activity defined as that required for the oxidation of 1 μmol NADH min^{-1} mg $protein^{-1}$ at 25 °C and pH 7.4.

2.7.2. Lactate dehydrogenase (LDH) activity

An aliquot of total cell protein extracts was incubated in 200 mmol l^{-1} Tris–HCl pH 7.4, 0.3 mmol l^{-1} NADH and 5 mmol l^{-1} pyruvate sodium. LDH reduces NAD to NADH at 340 nm and was calculated with one unit of activity defined as that required for the oxidation of 1 μmol NADH min^{-1} mg $protein^{-1}$.

2.8. Proton NMR spectroscopy

NMR spectroscopy was performed on a small-bore 500-MHz Bruker Avance DRX spectrometer equipped with a high resolution magic angle spinning (HRMAS) probe. Tumor or plasma samples were set into 4 mm-diameter, 50 μl, free-volume, zirconium oxide rotor tubes. Rotors were spun at 4 kHz and cooled at 4 °C, using the BCU-05 temperature unit. A one dimensional ^{1}H NMR spectrum was obtained using a nuclear Overhauser enhancement spectroscopy sequence with low-power water-signal presaturation (NOESYPR). Then, a two dimensional ^{1}H NMR spectrum was immediately recorded using a Total Correlation Spectroscopy (TOCSY) sequence. Spectra were processed using the Topspin 2.0 software package (Bruker, Karlsruhe, Germany).

2.8.1. Metabolomics

NOESYPR spectra were phased and baseline-corrected. Then, metabolite-related signals were quantified according to a previously published method [19,20]. TOCSY spectra were reconstructed at both high resolution (2048 × 256) for assignments and lower resolution (256 × 256) for quantification. After baseline correction, TOCSY spectra were transferred to the Excel database (Microsoft Co.). Quantification of metabolite-related cross-peak volumes (CPVs) was performed using a homebuilt routine [19,20].

2.8.2. Label-assisted metabolite profiling

Label-assisted metabolite profiling aims at identifying at steady-state derivatives having incorporated the ^{13}C label from a ^{13}C-labeled precursor [21]. Two subgroups of CTL (n = 3) and INH (n = 3) tumors

were exposed to DL-[1,2-^{13}C]glucose administered by intraperitoneal injection (10 mg in 200 μl). Thirty minutes after administration, the animals were sacrificed. Tumors were removed and prepared for analysis. NMR analyses were performed using a 2D ^{1}H–^{13}C heteronuclear multiple quantum coherence (HMQC) sequence with acquisition parameters given in a previous report [21]. HMQC spectra were exponentially filtered and baseline corrected. CPVs of interest were measured, and ratios of CPVs were used to calculate label incorporation [21].

2.9. Plasma biochemistry

Total mixed blood (arterial and venous) was collected in heparinated tubes, then centrifugated. Free thiol groups which reflect the oxidative status of sulfhydril aminoacids, thiobarbituric acid-reactive substances (TBARS), and malondialdehyde (MDA) which reflect lipid peroxidation were measured using assay kits according to the manufacturer's recommendations and spectrophotometric reading.

2.10. Transcriptomics

The analysis used the Taqman low-density array technique (Applied Biosystems) to screen 85 genes of interest encoding for: Bioenergetic metabolism, lipid/phospholipid metabolism, glutamate metabolism, oxidative stress, proliferation, apoptosis and DNA repair, Other cell stress responses and signaling, oncogenes and oncosuppressors and protein phosphatases 1 and 2 (Supporting Information Table 1).

2.11. Statistical analysis

Univariate comparison between groups was done using the Student's *t*-test and multivariate statistical analysis using partial least squares analysis. Statistical analyses were performed using the XLSTAT 2008 software (Addinsoft).

3. Results

3.1. Phenotype alterations in melanoma directly targeted by localized chemotherapy

3.1.1. Tumor weight

CTL tumors were collected from day 15 to day 20 after B16 cell inoculation with an average weight of 1.11 ± 0.66 g (1.58 ± 0.40 g specifically at day 20) (Fig. 2A). Fotemustine-treated tumors (INH) stopped proliferation after chemotherapy administration, with a tumor mass of 0.23 ± 0.06 g (day 15 to day 29 average, $P < 0.001$, INH vs CTL), then resumed reduced growth. Tumors recovering growth after chemotherapy (REC) had reduced weight of 0.85 ± 0.14 g (day 45 to day 57 average, $P < 0.05$, REC vs CTL). Kinetics of CTL, INH and REC tumor growth was previously reported [9], and showed that the major difference between CTL and REC tumors was the reduced tumor size in the latter, enabling long duration survival with an acceptable tumor burden (less than 10% of the animal body weight).

3.1.2. Metabolic analysis

Typical ^{1}H NMR spectra are displayed in Fig. 2B. In comparison with CTL tumors, INH tumor spectra exhibited decreased Lac and Succ content indicating bioenergetics reprogramming. REC tumor spectra showed unchanged Lac, decreased Succ, decreased GSx and increased PUF levels.

To confirm the reprogramming of glycolysis, we used label-assisted metabolite profiling aimed at identifying at steady-state derivatives having incorporated the ^{13}C label. Two groups of CTL and INH tumors were exposed to DL-[1,2-^{13}C]glucose administered *i.p.*

In comparison with unlabeled tumor spectra, CTL and INH tumors having incorporated DL-[1,2-^{13}C]glucose showed obvious labeling of Ala at positions C2 and C3, and Lac at positions C2 and C3. In comparison with CTL tumors, INH tumors showed accumulation of free unphosphorylated glucose (Fig. 2C and D) and decreased ^{13}C incorporation in Lac (×0.7 ± 0.1, $P < 0.05$). These changes in Glc and Lac labeling demonstrate downregulation of glycolysis in INH tumors. Also INH tumors showed Ser labeled at position C2. Ser is a product of glycolysis that accumulates probably due to diminished downstream consumption.

Other labeled metabolites included Gly at position C2 (×1.7, $P < 0.05$ INH vs CTL), Glu and Gln at position C3 and C4 (×3.1 and ×1.8 for Glu, and ×2.0 and ×3.5 for Gln, respectively, $P < 0.05$), and Asp at position C3 (×1.8, $P < 0.05$) (Fig. 2E). Labeled Glu, Gln and Asp in C3 and C4 originated from transamination of glucose-derived oxoacids of the Krebs cycle, testifying activation of the Krebs cycle.

Glycolysis was further investigated by measuring PK and LDH activities. PK activity was increased in INH tumors (0.30 ± 0.06 vs 0.66 ± 0.08 μmol min^{-1} mg protein^{-1}, INH vs CTL, $P < 0.01$) (Fig. 2F), while LDH activity was decreased (0.73 ± 0.25 vs 1.92 ± 0.34 μmol min^{-1} mg protein^{-1}, $P < 0.01$) (Fig. 2G).

Taken together, ^{1}H NMR spectra, ^{13}C-label-assisted metabolite profiling and enzyme activities demonstrated downregulation of glycolysis and upregulation of the Krebs cycle in INH tumors.

Proton-NMR spectroscopy-based metabolomics enabled quantification of 35 tumor metabolites, gathered into several metabolite subsets (Table 1).

In the *Bioenergetic metabolism* subset of INH tumors, Glc was increased (×18, $P < 0.05$) and Lac and Succ decreased (−25%, $P < 0.025$ and − 74%, $P < 0.001$, respectively). As reported in discussion, this combination was underpinned by downregulation of glycolysis and upregulation of the Krebs cycle. Curiously in the context of upregulation of mitochondrial activity and respiration, ATP levels were decreased (−32%, $P < 0.05$). In REC tumors, Succ was decreased by −43% ($P < 0.05$).

The *lipid/phospholipid metabolism* subset was markedly altered in all tumor groups. PtC was increased in INH and REC groups (+57% and +43% respectively $P < 0.05$), also PE (+90% and +53%, all $P < 0.05$), while GPC and GPE increased only in INH tumors by +148% and +82% (both $P < 0.001$).

The *glutamate metabolism* subset was markedly altered in INH tumors. All metabolites increased significantly (Gln × 3.8, Glu, +77%, Pro × 2.9, Asp × 4.3, Asn, ×5.2, all $P < 0.01$, and Arg × 3.7, Ala, +40%, both $P < 0.05$). These variations can be correlated with labeled assisted metabolite profiling of INH tumors. Only Gln and Asp remained elevated during the REC phase (Gln, +109%, and Asp, +142%, both $P < 0.025$).

The *oxidative stress metabolism* subset of INH tumors showed maintained GSx level but increased tCr level (+84%, $P < 0.01$). In contrast, REC tumors had decreased GSx (−24% $P < 0.05$) and unchanged tCr.

From this metabolomic analysis, INH tumors showed dominant alterations in bioenergetic metabolites (to which we may associate glutamate derivatives according to labeled-assisted metabolite profiling) and phospholipid metabolites (about 75% of class metabolites, Table 1). This pattern was also found in REC tumors.

3.1.3. Transcriptomic analysis

Transcriptional analysis was performed in 85 genes, gathered into several gene subsets (Table 2). Full names of genes and encoded proteins are given in Supporting Information Table 1.

In the *Bioenergetic metabolism* subset, the INH group displayed downregulation of Slc2a1, Pfk1, Tkt, and Pgk1, although upregulation of 6-phosphofructo-2-kinase (Pfkfb3). REC tumors showed upregulation of Pfkfb3, only.

In the *lipid/phosholipid metabolism* subset, INH tumors showed downregulation of Chka and Acly, and upregulation of Pla2r1, Pld2, Pcyt1a and Cept. Six transcripts among 17 from this subset were modified. In the REC group, there was downregulation of Fasn and upregulation of Pclb1, Pld2 and Cept1.

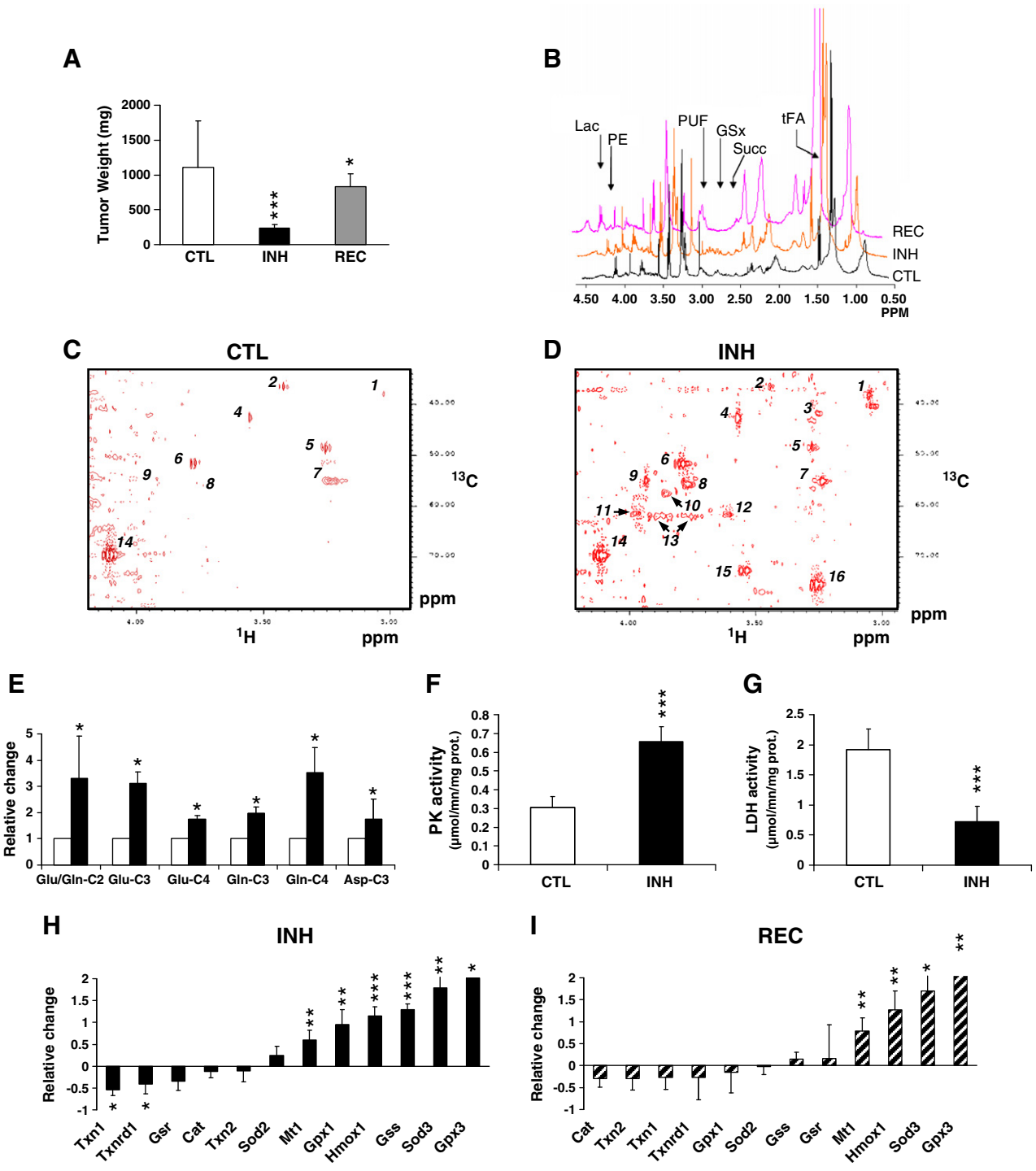

Fig. 2. Phenotype alterations in fotemustine-treated melanomas. A. Tumor weight in the 3 groups (CTL, INH, REC). White bar, CTL; black bar, INH; hatched, REC. Data are normalized to the CTL group values. *, $P < 0.05$; ***, $P < 0.01$, group vs CTL. B. Typical 1D HRMAS ^{1}H NMR spectra of tumors from the 3 groups (CTL, INH, REC). The displayed spectral range is 0.5–4.6 ppm. Black, CTL; red, INH, and purple, REC. Arrows, signals from indicated metabolites. For metabolite abbreviations, see Table 1. C,D. Typical HRMAS ^{13}C–^{1}H HMQC spectrum selections from CTL (C) and INH (D) tumors after incorporation and metabolism of DL-[1,2-^{13}C]glucose administered to mice by intraperitoneal injection. The spectral range is 2.80–4.40 ppm along the ^{1}H axis and 45–80 ppm along the ^{13}C axis. 2D signals are numbered from 1 to 16: 1, tCr CH_3; 2, Tau CH_2–S; 3, PE CH_2–N; 4, Gly CH_2; 5, Tau CH_2–N; 6, Ala (C2)H; 7, derivatives of Cho $N(CH_3)_3$; 8, Glu/Gln (C2)H; 9, tCr CH_2; 10, Ser (C2)H_2; 11, Ser (C3) H_2/PE CH_2–O; 12, PC CH_2–N; 13, Glc (C6)H; 14, Lac CH; 15, Glc (C2)α; 16, Glc (C2)β. For metabolite abbreviations, see Table 1. E. Quantification of ^{13}C incorporation in metabolites of the glutamate metabolism subset. White bar, HMQC signal level for all carbons was set to 1 in CTL tumors. Black bars, relative HMQC signal variation of specified carbons in INH tumors. For metabolite abbreviations, see Table 1. *, $P < 0.05$, INH vs CTL. F. Pyruvate kinase (PK) activity in CTL and INH tumors. Data are given in μmol mn^{-1} mg $protein^{-1}$. ***, $P < 0.01$, INH vs CTL. G. Lactate dehydrogenase (LDH) activity in CTL and INH tumors. Data are given in μmol mn^{-1} mg $protein^{-1}$. ***, $P < 0.01$, INH vs CTL. H,I. Oxidative stress response-related transcripts in INH (H) and REC (I) tumors classified by magnitude of variation. *, $P < 0.05$; **, $P < 0.025$; ***, $P < 0.01$, INH or REC vs CTL.

In the *glutamate metabolism* subset, the INH group showed upregulation of Gpt1. In the REC group, there was downregulation of Glul.

In the *oxidative stress metabolism* subset, INH tumors showed major variation in this class of transcripts, thus 8 among 12 transcripts were affected, such as downregulation of Txn1 and Txnrd1 and upregulation of Mt1, Hmox1, Sod3, Gpx1, Gpx3 and Gss (Fig. 2H). In REC tumors, there was upregulation of Mt1, Hmox1, Sod3, and Gpx3 (Fig. 2I).

Table 1
Metabolomics of tumor groups.

	CTL		INH		REC		BS	
	Mean	SD	Mean	SD	Mean	SD	Mean	SD
n	7		11		11		10	
Bioenergetic metabolism								
Glc	1	2.07	18.12	15.31*	4.00	2.96*	2.79	2.61
Lac	1	0.17	0.75	0.09**	1.03	0.08###	1.07	0.18
MyI	1	1.07	3.32	1.33***	3.08	1.18***	1.86	0.87$
Succ	1	0.37	0.26	0.07***	0.57	0.15*,#	0.64	0.11*
Fum	1	0.32	0.84	0.13	0.96	0.13	1.06	0.18
Ace	1	0.33	0.63	0.15*	1.38	0.22*,###	1.64	0.42
ATP	1	0.25	0.68	0.16*	0.98	0.13#	0.84	0.18
UDPX	1	0.23	1.04	0.12	0.88	0.10	0.77	0.08*
Lipid/phospholipid metabolism								
tFA	1	0.47	4.60	2.24*	3.94	1.51*	3.09	1.05*
PUF	1	0.53	2.23	1.06	3.08	0.90**	2.20	0.63*
Cho	1	0.70	1.84	0.61*	1.67	0.53	1.11	0.40$
PC	1	0.41	1.11	0.25	1.53	0.42	0.63	0.22
PtC	1	0.10	1.51	0.16***	1.43	0.14***	1.28	0.13*
GPC	1	0.53	2.48	0.63***	0.64	0.20###	0.46	0.21*
PE	1	0.23	1.90	0.17***	1.53	0.16***,###	1.48	0.22*
GPE	1	0.38	1.82	0.30***	0.89	0.15###	0.36	0.14***,$$$
Glutamate metabolism								
Gln	1	0.29	3.84	0.66***	2.09	0.36***,###	1.15	0.23
Glu	1	0.20	1.77	0.20***	0.96	0.09###	0.90	0.09
Asp	1	1.08	4.32	1.77***	2.42	0.97**,#	1.35	0.64$
Asn	1	0.87	5.21	1.75***	1.07	0.56###	0.55	0.28
Pro	1	1.05	2.93	1.44*	0.82	0.55#	0.52	0.40
Ala	1	0.18	1.40	0.14**	0.94	0.08###	0.86	0.07
Oxidative stress metabolism								
tCr	1	0.11	1.84	0.18***	1.08	0.08###	1.16	0.12
hTa	1	1.04	1.16	0.69	1.40	0.89	1.55	0.80**
Tau	1	0.06	0.93	0.05	1.12	0.08#	1.25	0.09
GSx	1	0.28	0.95	0.18	0.76	0.11*	0.69	0.08*
Arginine and glycine metabolism								
Arg	1	2.12	3.65	2.81*	0.56	0.47##	0.72	0.64
Ply	1	0.55	1.47	0.44	1.95	0.50**	1.24	0.48
Gly	1	0.14	1.18	0.12	1.12	0.12	1.05	0.09
DMG	1	0.96	12.67	5.30***	0.98	0.36###	0.72	0.25
For	1	0.42	0.93	0.34	1.13	0.20	1.12	0.29
Thr	1	0.49	1.71	0.48	0.62	0.11###	0.62	0.22
Other amino acid metabolism								
Leu	1	1.04	1.90	1.22	1.11	0.63	0.55	0.33
Lys	1	0.21	2.16	0.33***	0.95	0.09###	1.15	0.18
PA	1	1.09	3.73	1.63**	1.88	0.91#	1.21	0.52

Abbreviations: Glc, glucose; Lac, lactate; MyI, myoinositol; Succ, succinate; Fum, fumarate; Ace, acetate; ATP, adenosine triphosphate; UDPX, uridine–diphosphate conjugates; tFA, total free fatty acids; PUF, polyunsaturated fatty acids; Cho, choline; PC, phosphocholine; PtC, phosphatidylcholine; GPC, glycerophosphocholine; PE, phosphoethanolamine; GPE, glycerophosphoethanolamine; Gln, glutamine; Glu, glutamate; Asp, aspartate; Asn, asparagine; Pro; proline; Arg, arginine; Ala, alanine; hTa, hypotaurine; Tau, taurine; GSx, total glutathione (GSH + 2 × GSSG); tCr, total creatine (creatine + phosphocreatine); Ply, polyamines; Gly, glycine; For, formate; DMxG, dimethylglycine; Thr, threonine; Leu, leucine; Lys, lysine; PA, phenylalanine.
*, $P < 0.05$; **, $P < 0.25$; ***, $P < 0.01$, Tumor group vs CTL; #, $P < 0.05$; ###, $P < 0.01$, Tumor group vs INH; $, $P < 0.05$; $$$, $P < 0.01$, BS vs REC.

Other changes with INH tumors included downregulation of Trp53, upregulation of Mgmt, upregulation of Cdkn1a, downregulation of Kit and Myc, and upregulation of Fos, Hras1 and Jun. In REC tumors, there was downregulation of Casp3 and upregulation of Mgmt, downregulation of Kras and Myc and upregulation of Fos and Jun.

From this transcriptomic analysis, INH tumors showed regulations in genes encoding for bioenergetic metabolism, oxidative stress response (67% of subset genes, Table 2), proliferation and oncogenes, while, in REC tumors, gene expression variations were dominated by oxidative stress response (33% of subset genes) and other stress responses.

3.2. Localized chemotherapy does not injure normal tissue but severely impacts BS tumors

3.2.1. Normal tissue

To investigate BS responses to localized chemotherapy, we sought whether morphological features of normal organs were affected at distance from treated tumors.

The animal weight corrected for tumor mass decreased by 11 ± 5% in the INH group ($P < 0.05$) and 9 ± 11% (P = NS) in the REC group (Fig. 3A). The liver and the soleus muscle weight did not significantly vary in mice bearing INH or REC tumors (17 ± 17% and 16 ± 14%, P = NS, respectively, Fig. 3B and C). In addition, liver and muscle exhibited macroscopic features similar to organs collected from tumor-free mice.

These data indicate that localized chemotherapy of B16 melanomas did not damage normal tissues distant from the tumor site. However, due to differential vulnerabilities of normal and tumor tissues, in a second experiment, we re-inoculated at distance, in the opposite flank, B16 cells to obtain naive BS tumors which were further analyzed.

3.2.2. BS tumors

3.2.2.1. Tumor mass. Distant BS tumors had strongly reduced mass in comparison with CTL tumors (0.77 ± 0.37 g, day 45 to day 57 average, $P < 0.05$ BS vs CTL) (Fig. 3D). These data indicate that BS tumors, to the difference of healthy liver and skeletal muscle, respond to the presence of chemotherapy-treated tumors.

3.2.2.2. Histopathology. Representative color photographs of histological slices of tumors are given in Fig. 3E. As shown in Fig. 3F–J, INH tumors showed dramatic decrease in mitotic count (4.9 ± 3.7 vs 102.3 ± 13.2, INH vs CTL, $P < 0.01$), severe anisocytosis (rated 4.8 ± 0.4 vs 0.4 ± 0.5, $P < 0.01$) accompanied with hyperploid cells witnessing genomic instability, enlarged cytoplasm, features of decreased aggressiveness, low level of necrosis (rated 0.8 ± 1.0 vs 2.0 ± 0.8, $P < 0.025$), intense pigmentation (rated 3.6 ± 0.7 vs 0.9 ± 0.4, $P < 0.05$), and weak vascularization level (rated 0.7 ± 0.6 vs 1.7 ± 1.1, $P < 0.05$).

REC tumors exhibited decreased mitotic count (59.4 ± 19.1 vs 102.3 ± 13.2, REC vs CTL, $P < 0.01$), increased pigmentation load (rated 2.4 ± 1.2 vs 0.9 ± 0.4, $P < 0.01$), and anisocytosis (rated 1.7 ± 0.6 vs 0.4 ± 0.5, $P < 0.01$) (Fig. 3E–I).

BS tumors had significantly decreased mitotic count (70 ± 17 vs 102.3 ± 13.2, BS vs CTL, $P < 0.01$), and increased melanin content (rated 2.5 ± 1.7 vs 0.9 ± 0.4, BS vs. CTL, $P < 0.025$) as shown in Fig. 3E, F and I.

BS tumors showed several histological features in common with REC tumors, although they had never been in contact with chemotherapy, but lower level of anisocytosis.

Interestingly, the amount of tumor infiltrating lymphocytes (TIL) was similar in all groups (Fig. 3G–K), and no sign of inflammation was seen in histopathology slices, in favor that the model did not implicate substantial immunogenic mechanism.

Thus, in contrast to investigated normal tissues, BS tumors responded to the presence of treated tumors at distance.

3.2.2.3. Metabolomic analysis. Proton-NMR spectra of BS tumors showed, in comparison with CTL tumors, unchanged Lac but still decreased Succ level. GSx was decreased and PUF increased in a similar manner than REC tumors (Fig. 4A).

In the *bioenergetic metabolism* subset of BS tumors, Succ was decreased (−36%, $P < 0.05$) and UDPX was decreased (−23%, $P < 0.05$). (Table 1). Succ and pyrimidine precursors are intermediates synthesized into mitochondria, which suggests the targeting of mitochondria in BS tumors.

Like in fotemustine-treated tumors, the *lipid/phospholipid metabolism* subset was altered in BS tumors. PtC and PE were increased

Table 2
Transcriptomics of tumor groups.

	CTL		INH		REC		BS	
	Mean	SD	Mean	SD	Mean	SD	Mean	SD
n	4		3		4		4	
Bioenergetic metabolism								
Slc2a1	1	0.24	0.35	0.17**	1.59	1.03#	1.28	0.52
Hk2	1	0.16	0.69	0.43	0.94	0.60	1.20	0.20
Pfkl	1	0.22	0.50	0.19*	0.72	0.26	1.09	0.27
Pfkm	1	0.23	1.18	0.17	0.96	0.47	1.16	0.33
Pfkfb3	1	0.24	1.73	0.26**	1.77	0.17**	1.51	0.48
Tkt	1	0.27	0.47	0.10**	0.78	0.53	1.33	0.31
Pgk1	1	0.26	0.48	0.21*	0.74	0.43	1.41	0.40
Pkm2	1	0.18	0.88	0.41	1.09	0.42	1.55	0.45
Ldha	1	0.36	0.83	0.53	1.24	0.27	0.85	0.38
Ldhb	1	0.31	1.61	0.58	0.77	0.50#	1.39	0.27
Mdh1	1	0.32	1.23	0.70	0.79	0.55	1.28	0.38
Mdh2	1	0.25	1.02	0.32	0.81	0.42	1.60	0.48$
Aco1	1	0.28	0.81	0.22	0.71	0.49	1.43	0.29$
Hif1a	1	0.41	0.75	0.23	1.00	0.29	1.50	0.55
Lipid/phospholipid metabolism								
Pla2g6	1	0.26	0.96	0.23	0.68	0.30	1.38	0.41$
Pla2r1	1	0.41	1.89	0.60*	1.07	0.39#	1.66	0.72
Plcb1	1	0.52	1.79	0.60	2.46	1.16*	1.12	0.45
Plcb3	1	0.40	0.93	0.56	0.69	0.20	1.54	0.56$
Plcd1	1	0.28	1.00	0.24	1.37	0.53	1.70	0.65
Plch1	1	0.45	1.51	1.25	0.74	0.48	1.22	0.43
Pld1	1	0.46	1.37	0.22	1.17	0.37	1.67	0.71
Pld2	1	0.19	5.67	1.29**	2.49	0.88*,##	1.05	0.18$
Chka	1	0.28	0.52	0.06*	0.72	0.31	1.06	0.16
Chkb	1	0.29	0.92	0.12	0.82	0.10	1.25	0.37
Pcyt1a	1	0.25	1.42	0.25*	1.10	0.43	1.48	0.43
Pcyt1b	1	0.36	1.16	0.25	0.87	0.38	1.39	0.73
Cept1	1	0.42	5.23	4.16*	2.57	0.82*	0.95	0.61$
Etnk1	1	0.29	1.30	0.19	0.97	0.69	1.35	0.34
Pemt	1	0.35	0.66	0.37	0.67	0.47	1.10	0.23
Acly	1	0.38	0.53	0.11*	0.66	0.48	1.53	0.55
Fasn	1	0.34	0.65	0.16	0.52	0.34*	1.34	0.36$
Glutamate metabolism								
Gls	1	0.33	0.73	0.19	0.81	0.55	1.44	0.39
Glul	1	0.29	0.81	0.17	0.44	0.14*,#	1.34	0.31$
Got1	1	0.24	1.10	0.36	0.68	0.42	1.54	0.34
Got2	1	0.27	0.84	0.27	0.73	0.51	1.53	0.44
Gpt1	1	0.14	2.07	0.70*	1.27	0.83	0.85	0.18$$
Oxidative stress								
Hmox1	1	0.28	2.15	0.20***	2.27	0.43**	1.77	0.67
Txnrd1	1	0.21	0.58	0.22*	0.73	0.52	1.18	0.23
Txn1	1	0.42	0.45	0.13*	0.73	0.28	0.52	0.20
Txn2	1	0.31	0.89	0.25	0.70	0.26	1.35	0.32$
Sod2	1	0.29	1.25	0.20	0.98	0.18	1.69	0.53*,$
Sod3	1	0.68	2.79	0.56**	2.71	1.48*	0.93	0.38$
Gpx1	1	0.29	1.95	0.33**	0.85	0.47#	1.68	0.53*,$
Gpx3	1	0.39	10.22	9.06*	11.52	8.82*	2.62	1.04*
Gsr	1	0.34	0.65	0.20	1.16	0.77	2.21	0.70*
Gss	1	0.32	2.29	0.14***	1.15	0.16###	1.42	0.35
Cat	1	0.32	0.88	0.15	0.70	0.19	1.27	0.39$
Mt1	1	0.11	1.59	0.23**	1.78	0.30**	1.46	0.38*
Proliferation, apoptosis and DNA repair								
Mgmt	1	0.48	15.33	8.63*	15.63	5.40***	1.76	0.56$
Trp53	1	0.33	0.59	0.17*	0.65	0.32	1.51	0.44$
Bcl2	1	0.39	1.39	0.37	0.82	0.26#	1.54	0.42$
Bax	1	0.27	1.19	0.13	0.63	0.23##	1.40	0.39$
Casp3	1	0.31	0.99	0.12	0.54	0.28*,#	1.26	0.35$
Ccnd1	1	0.36	1.41	0.68	1.10	0.50	1.52	0.50
Cdkn1a	1	0.33	3.51	0.32***	1.37	0.22###	1.25	0.41
Cdkn1b	1	0.23	0.82	0.07	0.96	0.69	1.26	0.33
Cdkn2a	1	0.98	1.16	0.82	2.28	1.25	1.63	0.41
Other cell stress responses and signaling								
Mitf	1	0.39	0.85	0.39	0.58	0.44	1.32	0.47$
Tyr	1	0.31	1.52	0.55	1.23	0.80	1.45	0.17*
Mdm2	1	0.41	2.81	0.65**	1.00	0.56##	1.57	0.55
Rb1	1	0.37	2.17	0.41**	0.96	0.30##	1.44	0.55
Mia1	1	0.68	0.35	0.05	0.77	0.61	0.96	0.51
Pcna	1	0.30	0.42	0.17*	0.54	0.41	1.47	0.43$
Other cell stress responses and signaling								
Prkaca	1	0.31	0.96	0.20	0.68	0.16#	1.27	0.31$
Tert	1	0.53	0.86	0.37	0.76	0.61	0.71	0.22
Oncogenes and oncosuppressors								
Akt1	1	0.31	0.89	0.34	0.80	0.50	1.43	0.35
Fos	1	0.28	2.61	0.36***	2.85	0.57***	1.40	0.69$
Hras1	1	0.29	1.66	0.43*	0.90	0.42#	1.43	0.33
Jun	1	0.44	2.04	0.60*	1.91	0.32*	1.04	0.33$
Kit	1	0.24	0.41	0.27*	0.61	0.47	0.73	0.39
Kras	1	0.32	0.70	0.18	0.63	0.12*	0.61	0.12*
Myc	1	0.35	0.26	0.10*	0.46	0.30*	1.43	0.46$
Nras	1	0.33	0.90	0.21	0.84	0.51	1.64	0.46*
Raf1	1	0.31	0.87	0.25	0.87	0.65	1.31	0.39
Pten	1	0.30	1.35	0.28	0.79	0.48	1.41	0.46
Stk11	1	0.29	1.12	0.08	0.99	0.31	1.50	0.39
Protein phosphatases 1 and 2								
Ppp1ca	1	0.29	0.68	0.10*	0.54	0.24*	1.39	0.31$
Ppp1cb	1	0.38	0.76	0.25	0.63	0.51	1.18	0.30
Ppp2ca	1	0.22	0.94	0.21	0.87	0.46	1.37	0.35
Ppp2cb	1	0.27	0.83	0.16	0.87	0.65	1.38	0.35
Ppp2r1a	1	0.30	0.81	0.24	0.55	0.27*	1.28	0.24$
Ppp2r1b	1	0.39	0.90	0.14	0.79	0.42	1.57	0.52$
Ppp2r5c	1	0.30	0.74	0.14	0.73	0.32	1.63	0.50$
Lcmt1	1	0.25	0.82	0.06	0.66	0.24	1.21	0.20$
Ppme1	1	0.24	0.68	0.24	0.79	0.39	1.38	0.43

Genes, see Supplementary Table 1. *, $P < 0.05$; **, $P < 0.25$; ***, $P < 0.01$, Tumor group vs CTL; #, $P < 0.05$; ##, $P < 0.025$, ###, $P < 0.01$, Tumor group vs INH; $, $P < 0.05$; $$, $P < 0.025$, BS vs REC.

(+43% and +48%, respectively, both $P < 0.05$). In contrast to the INH group, GPC and GPE were decreased in BS tumors (−54% and − 64%, respectively, $P < 0.05$). Total fatty acid (tFA) levels were increased, as in INH and REC tumors, by 209%, $P < 0.05$, as well as polyunsaturated fatty acids (PUF) by +120%, $P < 0.05$.

In the *Glutamate metabolism* subset no change was found in BS tumors. In contrast, in the *Oxidative stress metabolism* subset, BS tumors showed a strong decrease of GSx (−39% $P < 0.05$) and an increase of Tau (+25%, $P < 0.025$).

Metabolomic analysis revealed that BS tumors displayed changes mainly in phospholipid and oxidative stress metabolism (75% and 50% of subset metabolites, respectively, Table 1).

3.2.2.4. Transcriptomic analysis. In contrast with fotemustine-treated tumors, BS tumors had less pronounced gene expression changes (Table 2).

The most regulated gene subset in BS tumors was that of *Oxidative stress response*, including Gpx3 (×2.6), Gsr (×2.2) and Sod2 (×1.7), Gpx1 (+68%), and Mt1 (+46%), all $P < 0.05$ (Fig. 4B). Otherwise, there was upregulation of Tyr (+45%), and proto-oncogene expression changes with downregulation of Kras and upregulation of Nras (−39% and +64%, respectively, both $P < 0.05$).

Overall, transcriptional analysis of BS tumors showed alteration of genes involved in cellular oxidative stress response and ras oncogene family. Because Sod2 is specifically mitochondrial, and Gsr mostly expressed in mitochondria, we conclude that mitochondria was probably a target in BS effect.

3.2.2.5. Integration of metabolomics and transcriptomics. Multivariate statistical analysis was applied to metabolomics and transcriptomics data of CTL, REC and BS tumors, to help revealing global features of BS response. INH tumors were excluded of this analysis because these tumors would have severely weighted the analysis with the reversal of Warburg effect.

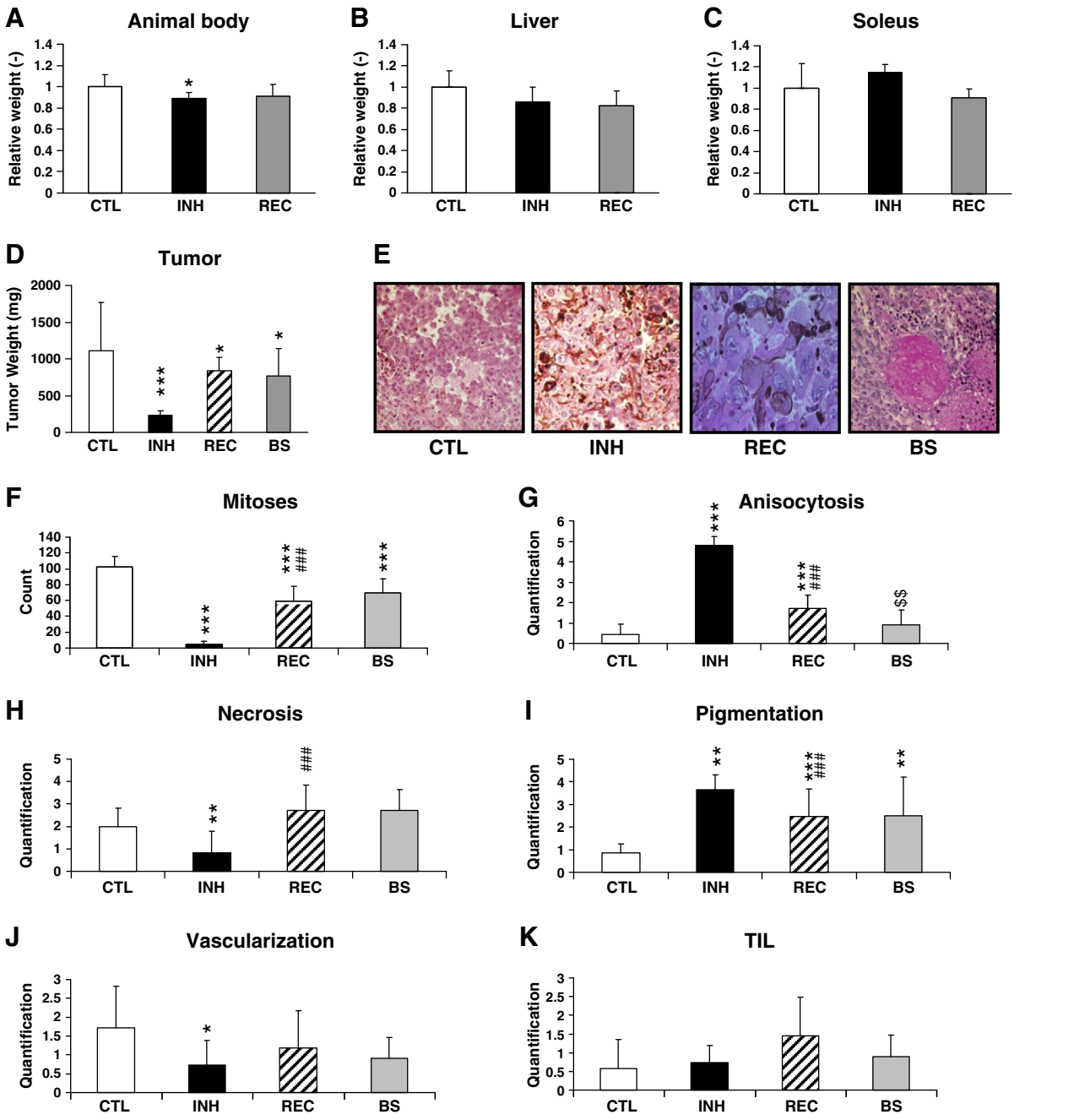

Fig. 3. Morphological alterations in distant normal tissues and BS tumors. A–C. Morphological features of distant normal tissues in mice bearing a treated tumor. Weights are normalized to the CTL value. Body weight with tumor weight subtracted (A), liver (B), and soleus muscle (C).*P < 0.05 INH vs CTL. D. Tumor weight in 4 groups. White bar, CTL; black bar, INH; hatched, REC; gray, BS. Data are normalized to the CTL group value. *, P < 0.05; ***, P < 0.01, group vs CTL. E—Photographs of histological slices (×40 magnification) of representative tumors from all groups (CTL, INH, REC and BS), showing features quantified below. CTL tumors show abundant mitoses and vasculature with numerous intravascular red blood cells. INH and REC tumors display poor microvessel density, and areas of anisocytosis and pigmentation. BS tumors exhibit decreased mitoses and areas of pigmentation . F–K. Histology of tumor groups. White bar, CTL; black bar, INH; hatched, REC; gray, BS. Data are normalized to the CTL group value. Mitotic count (F), anisocytosis (G), necrosis (H), pigmentation (I), vascularization (J) and tumor infiltrating lymphocytes (TIL) (K). *, P < 0.05; **, P < 0.025;***, P <0.01, tumor group vs CTL. ###, P < 0.01, tumor group vs INH; $$, P < 0.025 BS vs. REC.

Partial least squares analysis clusterized tumor samples into well separated groups, thus enabling to identify the F2 vertical axis in both analyses as a BS effect axis, from intense effect (bottom, distant BS tumors) to weak effect (top, CTL tumors) (Fig. 4C and E).

The loading plot of metabolites showed that the F2 axis opposed tCr and Tau to GPE, GPC, GSx, Asn and Ala (Fig. 4D). In this analysis, the metabolic signature of the "pure" BS effect included high levels of tCr and Tau, and low levels of GPE, GPC, GSx, Asn and Ala. The corresponding biochemical phenotype was consistent with response to oxidative stress and detoxification (glutathione consumption and biosynthesis through transsulfuration, high level of Tau).

Based on this interpretation of the F2 axis, and group barycentre projection onto the F2 axis, it may be estimated that REC tumors contained about 40% of tumor cells responding through a proximal BS effect.

The loading plot of transcript expression showed that the F2 axis opposed Cdkn1a, Nras, Gsr, Aco1, Gss, and Ccnd1 to Kras (Fig. 4F). In this analysis, BS effect was characterized by upregulated response to oxidative stress (Gsr and Gss), and balanced expression of oncogenic ras isoform genes (upregulated Nras and downregulated Kras).

Here also, based on the interpretation of the F2 axis of transcript expression analysis, and group barycentre projection onto the F2 axis, it may be estimated that REC tumors contained about 46% of tumor cells

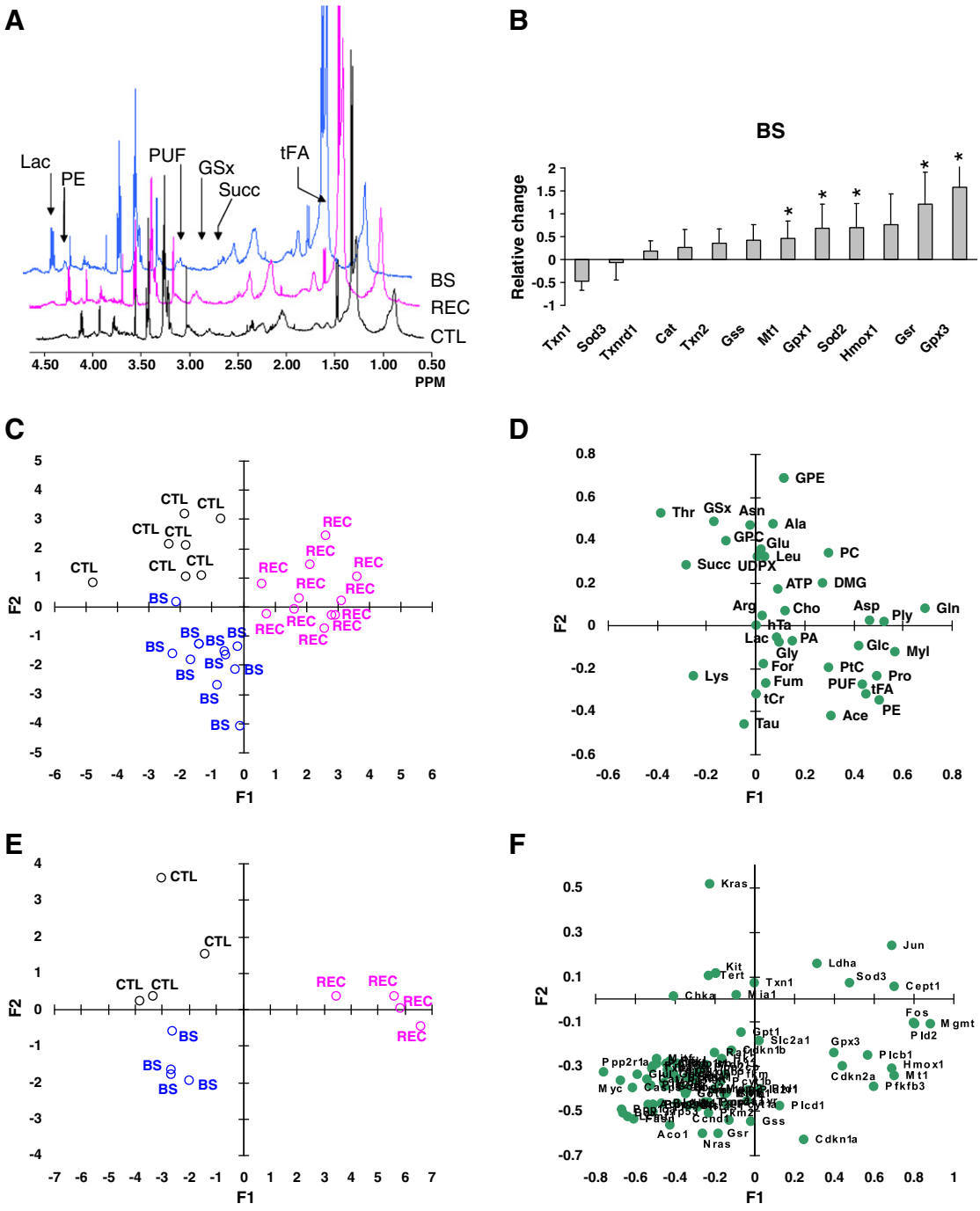

Fig. 4. Phenotype alterations in BS tumors and data integration. A. Typical 1D HRMAS ^{1}H NMR spectra of tumors from 3 groups (CTL, REC, BS). The displayed spectral range is 0.5–4.6 ppm. Black, CTL; purple, REC, and blue, BS. Arrows, signals from indicated metabolites. For metabolite abbreviations, see Table 1. B. Oxidative stress response-related transcripts in BS tumors, classified by magnitude of variation. *, $P < 0.05$, BS vs CTL. C, D. Partial least squares analysis of tumor metabolomic data. In this analysis, partial least squares coefficients of regression were R2X = 0.45 with metabolites and R2Y = 0.59 with groups. Plot of individual samples from the 3 groups (C). Black, CTL; purple, REC, and blue, BS. Loading plot (D). For metabolite abbreviations, see Table 1. E, F. Partial least squares analysis of tumor transcriptional data. In this analysis, partial least squares coefficients of regression were R2X = 0.50 with metabolites and R2Y = 0.88 with groups. Plot of individual samples from the 3 groups (C). Black, CTL; purple, REC, and blue, BS. Loading plot (D). For transcript abbreviations, see Supporting Information Table 1.

responding through a proximal BS effect, in excellent agreement with multivariate statistical analysis of metabolic data.

3.3. Serum of mice bearing treated tumors vehicles oxidative stress-related species

We previously showed that administration of serum from fotemustine-treated tumor-bearing mice as donors markedly inhibited tumor growth of untreated B16 melanoma (−77 ± 19%, $P < 0.001$, INH vs CTL sera) (Fig. 5A).

Because of this response and induction of oxidative stress response in BS tumors, we sought for biological markers in the plasma of treated tumor-bearing mice.

3.3.1. Global metabolic profile

Semi-quantitative analysis of NMR spectra was performed on sera of mice from CTL, INH, and REC groups (Fig. 5B). Glc and Gln plasma levels were similar in all groups. In the INH group, Lac and Ala levels were decreased, and Ace and Sarc levels increased. In the REC group, Lac and Succ levels were still decreased. Two-dimensional ^{1}H NMR

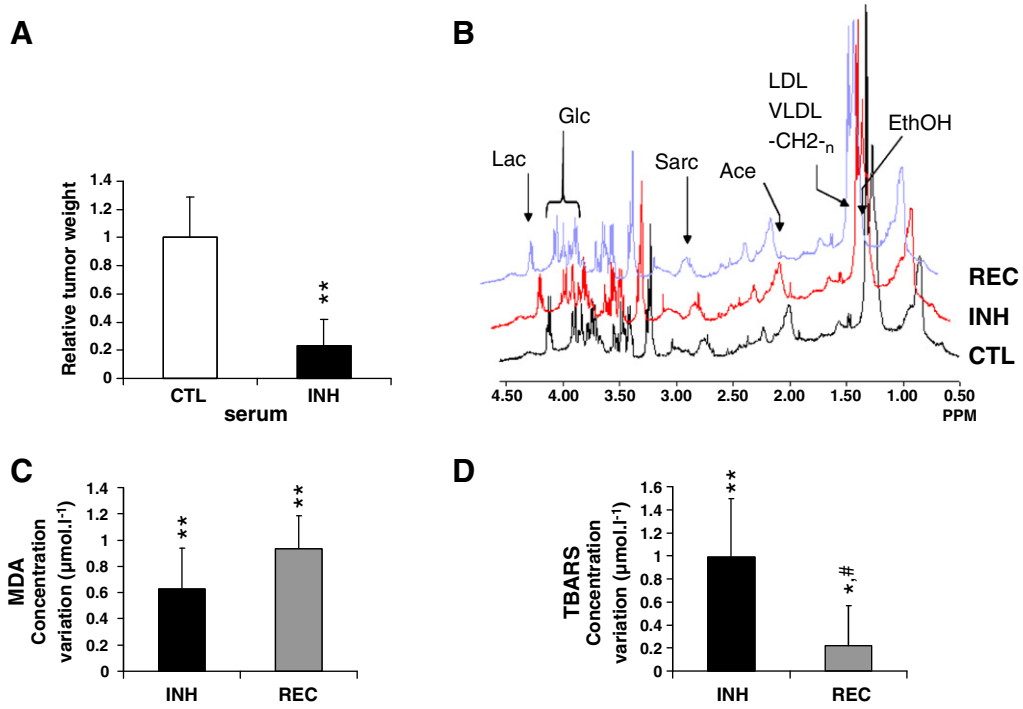

Fig. 5. Plasma of mice bearing treated tumors vehicles oxidative stress-related species. A. Effect on naïve B16 melanoma of administration of sera from mice bearing untreated tumors (white bar, CTL) or chemotherapy-treated tumors (black bar, INH). **, $P < 0.025$, INH vs CTL sera. B. Typical HRMAS ^{1}H NMR spectra of plasmas from CTL, INH and REC recipients. The displayed spectral range is 0.5–4.6 ppm. Black, CTL; red, INH, and indigo, REC. Arrows, signals from indicated metabolites. EthOH, ethanol; Sarc, sarcosine; LDL VLDL $(-CH_2-)_n$, lateral chain signals of fatty acids from LDL and VLDL plasma lipoproteins. For other metabolite abbreviations, see Table 1. C, D. Biochemistry of plasma. Malondialdehyde (C) and TBARS (D) concentration variation (µmol l^{-1}) in the plasma of INH and REC recipients, in comparison with the plasma of CTL recipients. *, $P < 0.05$; **, $P < 0.025$, recipient group vs CTL recipient; #, $P < 0.05$, REC recipient vs INH recipient.

spectroscopy of serum showed increased level of ethanol in the INH group (not shown). These data indicate that serum Lac may be related to mouse tumor burden, and that sera collected oxidative stress-related species (ethanol).

3.3.2. Biochemistry

Biochemical biomarkers of oxidative stress were measured in the 3 recipient groups of the first experiment (Fig. 5C and D). MDA was significantly increased in the serum of INH and REC tumor-bearing mice ($+0.63 \pm 0.30$ and $+0.93 \pm 0.25$ µmol l^{-1} vs CTL, both $P < 0.01$). TBARS were significantly increased in the plasma of INH and REC tumor-bearing mice ($+0.99 \pm 0.50$ and $+0.44 \pm 0.35$ µmol l^{-1}, $P < 0.01$ and $P < 0.05$ respectively). Protein thiols were similar in all recipient groups (P = NS). Thus the serum of treated tumor-bearing mice contained increased levels of oxidative stress-related derivatives.

4. Discussion and conclusions

In this article, we used a model of localized chemotherapy (*i.t.* administration of fotemustine), and sought whether it induced BS effect in distant normal tissue and untreated melanoma. Normal tissue in this study did not significantly respond to the presence of treated tumors. Then, we investigated whether BS tumors responded to localized chemotherapy of pre-implanted tumors. We found that BS tumors, to the contrary of normal tissues, strongly responded with reduced proliferation and severe oxidative stress response. This apparent discrepancy may be related to the fact that sensitivity to BS effects could depend on the level of replicative and transcriptional activities [22].

To help elucidating the mechanisms of chemotherapy-induced BS effect in vivo, we analyzed BS tumors and tumors receiving localized chemotherapy using an approach devoid of preconception and increasingly used to get a comprehensive view of phenotype changes, involving metabolic and transcriptional molecular screening.

During inhibition of proliferation, INH tumors exhibited strong genomic instability and showed evidence of a switch from glycolysis to Krebs cycle and oxidative phosphorylation. First, at the transcriptional level, we found downregulation of glycolysis-related genes including Slc2a1, Pfk1, Tkt and Pgk1. Second, at the metabolome level, we confirmed downregulation of glycolysis with decreased Lac level, decreased ^{13}C incorporation from Glc into Lac, and activation of the Krebs cycle, attested by strong decrease in Succ, and increased ^{13}C incorporation from Glc into Glu, Gln and Asp [23]. Succ was reported to stabilize transcription factor HIF1α, which in turn induces transcription of glycolysis-related genes [24]. Most of these bioenergetics disorders recovered in REC tumors.

An unexpected finding was ATP decrease, which was not likely related to decreased production in INH tumors that exhibit upregulated OXPHOS. Some explanations may be proposed for increased needs or losses of ATP in INH tumors. First, a recent finding was ATP secretion by chemotherapy-treated tumor cells [25], a mechanism that may induce a local immune response [26]. However, our histological data about TIL and inflammation do not agree with a significant role for immune response. Second, ATP consumption may be increased in treated tumor due to DNA repair, oxidative stress response and apoptosis.

Furthermore, INH tumors showed downregulation of acetyl-CoA-lyase (Acly), suggesting that the Krebs cycle worked and retained its intermediates, and downregulation of choline-kinase A (Chka) in favor of reduced aggressiveness [27]. Other genes of phospholipid metabolism were upregulated (including members of phospholipase A2 and D families, the former possibly explaining increased GPC and GPE values). An unexpected finding was the accumulation of PE, which may be linked to serine accumulation, a product of glycolysis, demonstrated by ^{13}C experiments. In addition INH tumors accumulated fatty acids,

possibly because the Krebs cycle was sufficiently fed with pyruvate from glycolysis, and did not require beta-oxidation of lipids.

In tumors resuming growth (REC tumors), most lipid metabolism-related genes recovered, but fatty acid synthase (Fasn) was downregulated. Fasn behaves as an oncogenic protein [28]. However, total free fatty acids, including PUF, accumulated, which could be related to either low level of beta-oxidation or lipid droplet formation [29].

In BS tumors, whereas glycolysis was not significantly altered, Succ was decreased as well as UDPX, a pyrimidine derivative. Because these metabolites or their precursors are synthesized within mitochondria, these alterations suggest targeting of mitochondrial functions in BS response. The hypothesis was reinforced by findings that BS tumors exhibit oxidative stress response implicating proteins of mitochondrial origin, and ras expression abnormalities [30], as discussed below.

Also, in BS tumors, lipid metabolism-related gene expression was not altered. However, tFA and PUF accumulated, possibly because of inhibition of beta-oxidation or lipid droplet formation. GPC and GPE decreased, to the difference of what was found in INH, REC and CTL tumors, and this finding may relate to differential response of members of phospholipase A2 family. From the PLS analysis, GPC and GPE were candidate biomarkers of BS response.

Oxidative stress response was the prominent common feature of INH, REC and BS tumors. In INH tumors, Tnx1 and Txnrd1 were downregulated. The thioredoxin system plays a role in control of proliferation, redox state and apoptosis. Other genes encoding for oxidative stress response (Hmox1, Sod3, Gpx1, Gpx3, Gss and Mt1) were upregulated. Gss was upregulated testifying GSH biosynthesis. In INH tumors, the antioxidant response implicated cytosolic enzyme activities.

In REC tumors, Hmox1, Sod3, Gpx3 and Mt1 were upregulated, showing that these tumors undergo oxidative stress probably due to sustained DNA damage and genomic instability. In these tumors, GSx decreased, a feature probably mediated by plasma membrane efflux transport and multidrug resistance proteins.

In BS tumors, a clear antioxidant response was elicited that differed from that of treated tumors. Upregulated genes were Gpx1 and Gpx3, Sod2, the latter encoding for an isoform of superoxide dismutase localized in mitochondria, and Gsr encoding glutathione reductase also present in mitochondria. GSx was decreased indicating involvement of detoxification processes. Therefore, oxidative stress response in BS tumors, to the difference of INH and REC tumors, involved a mitochondrial component. This is in line with bioenergetic metabolome abnormalities in BS tumors in favor of mitochondrial targeting, as previously discussed.

An unexpected finding in BS tumors was downregulation of Kras and upregulation of Nras. Ras oncogenes comprise the most frequently mutated class of oncogenes in melanomas, and the 3 isoforms, Hras, Kras and Nras, have functions in trafficking, localization and signaling.

It has been reported that both Nras and Kras were constitutively associated with different compartments of mitochondria, and implicated in mitochondrial morphology [31]. In addition, N-Ras was an essential component of the retrograde signaling system between the mitochondria and nucleus.

Kras expression was shown to alter nuclear gene expression encoding for mitochondrial proteins especially bioenergetic metabolism yielding increased dependence on glycolysis [32]. It is also associated to inhibition of Complex I of electron chain transport, which, in turn, may yield increased activity of Complex II-based respiration. Complex II activity is in competition for ubiquinone with dihydroorotate dehydrogenase, the mitochondrial key enzyme of pyrimidine synthesis. Such a mechanism could explain the metabolic phenotype of BS tumors including decreased levels of Succ and UDPX to sustain mitochondrial ATP production, at the expense of pyrimidine derivative synthesis.

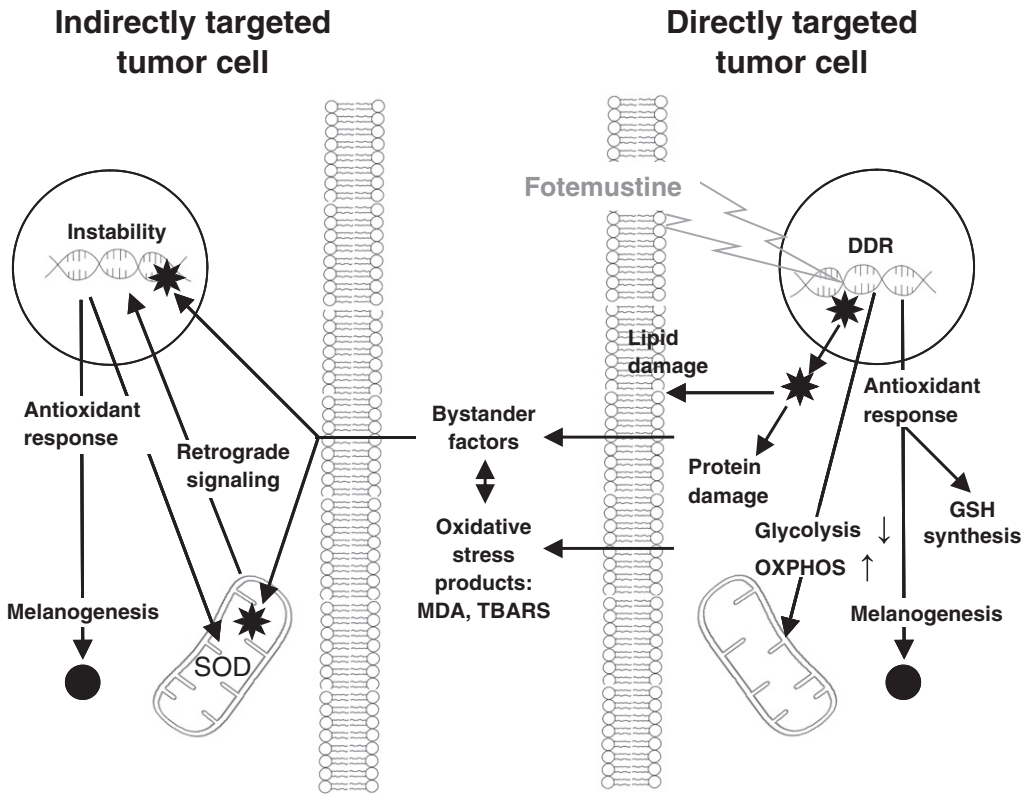

Fig. 6. Summary on chemotherapy-induced BS effect. Main findings and supported hypotheses on chemotherapy-induced BS effect. Star, reactive oxygen species. DDR, DNA damage response; MDA, malondialdehyde; TBARS, thiobarbituric acid-reactive substances; SOD, mitochondrial superoxide dismutase; GSH, reduced glutathione; ↓, downregulation; ↑, upregulation.

Taken together, combined alteration in Kras and Nras gene expression in BS tumor cells was in favor that mitochondria were major targets in response to BS factors. This adds to other findings about the involvement of mitochondria in response to BS factors, including increased oxidative stress response in mitochondria, and mitochondria-related bioenergetic metabolism alterations. To our knowledge, our data are the first to establish mitochondrial involvement in chemotherapy induced-BS effect in vivo.

A summary of our findings is given in Fig. 6. We propose that BS factors target nuclear and/or mitochondrial DNA, and induce genetic instability, as reported in response to radiation-induced BS factors [33,34]. Due to mitochondrial damage, BS tumor cells elicit retrograde signaling between mitochondria and nucleus. This triggers antioxidant response. Also, we show that the plasma of chemotherapy-treated mice contained increased level of oxidative stress-related species, which are candidate mediators of genetic instability and oxidative stress response in BS tumor cells.

Another important result of this study was based on multivariate statistical analyses of metabolomics and transcriptomics data. In these analyses, an axis could be interpreted as the BS effect axis. With metabolomics, the BS phenotype involved response to oxidative stress and detoxification. With transcriptomics, the BS phenotype was characterized with response to oxidative stress and ras oncogene expression changes (upregulation of Nras, and downregulation of Kras). Based on the identification of a BS effect axis, we could estimate the proportion of tumor cells undergoing proximal BS effect within the chemotherapy-treated tumor to 40–46%. BS effect was reported to occur in and out of the radiotherapy field [35], in agreement with our findings in tumors receiving localized chemotherapy and BS tumors. Our estimates of the BS contribution are in agreement with the proportion of cells undergoing BS effect in in vitro radiotherapy studies [36]. However, it is the first time that this contribution was estimated in vivo.

It is concluded from this study that localized chemotherapy induces severe oxidative stress response in BS tumors, but that normal tissues are spared by this effect. Therefore chemotherapy-induced BS effect may be a new mechanism in vivo by which chemotherapies as well as targeted therapies, may cause oxidative stress-related systemic effects such as chronic toxicity, metabolic diseases and oncogenesis.

This study also proposes an approach to evaluate the contribution of BS effect within treated tumors, and identifies the BS effect as a significantly contributing response to chemotherapy that may be exploited to improve overall response to cancer treatment.

Supplementary data to this article can be found online at http://dx.doi.org/10.1016/j.bbagen.2013.11.022.

Grant support

Institut National de la Santé et de la Recherche Médicale.

Author contributions

Conceived and designed experiments: DM, AD. Performed the experiments: DM, AD. Analyzed the data: DM, AD. Wrote the paper: DM, AD.

References

[1] J.B. Little, Genomic instability and bystander effects: a historical perspective, Oncogene 22 (2003) 6978–6987.
[2] L. Huang, A.R. Snyder, W.F. Morgan, Radiation-induced genomic instability and its implications for radiation carcinogenesis, Oncogene 22 (2003) 5848–5854.
[3] H. Nagasawa, J.B. Little, Unexpected sensitivity to the induction of mutations by very low doses of alpha-particle radiation: evidence for a bystander effect, Radiat. Res. 152 (1999) 552–557.
[4] I. Koturbash, J. Loree, K. Kutanzi, C. Koganow, I. Pogribny, O. Kovalchuk, In vivo bystander effect: cranial X-irradiation leads to elevated DNA damage, altered cellular proliferation and apoptosis, and increased p53 levels in shielded spleen, Int. J. Radiat. Oncol. Biol. Phys. 70 (2008) 554–562.
[5] M. Mancuso, E. Pasquali, S. Leonardi, S. Rebessi, M. Tanori, P. Giardullo, F. Borra, S. Pazzaglia, C.C. Naus, V. Di Majo, A. Saran, Role of connexin43 and ATP in long-range bystander radiation damage and oncogenesis in vivo, Oncogene 30 (2011) 4601–4608.
[6] M. Mancuso, E. Pasquali, S. Leonardi, M. Tanori, S. Rebessi, V. Di Majo, S. Pazzaglia, M.P. Toni, M. Pimpinella, V. Covelli, A. Saran, Oncogenic bystander radiation effects in Patched heterozygous mouse cerebellum, Proc. Natl. Acad. Sci. U. S. A. 105 (2008) 12445–12450.
[7] D.P. Kingsley, An interesting case of possible abscopal effect in malignant melanoma, Br. J. Radiol. 48 (1975) 863–866.
[8] P.J. Wersall, H. Blomgren, P. Pisa, I. Lax, K.M. Kalkner, C. Svedman, Regression of non-irradiated metastases after extracranial stereotactic radiotherapy in metastatic renal cell carcinoma, Acta Oncol. 45 (2006) 493–497.
[9] A. Demidem, D. Morvan, J. Papon, M. De Latour, J.C. Madelmont, Cystemustine induces redifferentiation of primary tumors and confers protection against secondary tumor growth in a melanoma murine model, Cancer Res. 61 (2001) 2294–2300.
[10] A. Demidem, D. Morvan, J.C. Madelmont, Bystander effects are induced by CENU treatment and associated with altered protein secretory activity of treated tumor cells: a relay for chemotherapy? Int. J. Cancer 119 (2006) 992–1004.
[11] J. Alexandre, Y. Hu, W. Lu, H. Pelicano, P. Huang, Novel action of paclitaxel against cancer cells: bystander effect mediated by reactive oxygen species, Cancer Res. 67 (2007) 3512–3517.
[12] S. Kohsaka, K. Takahashi, L. Wang, M. Tanino, T. Kimura, H. Nishihara, S. Tanaka, Inhibition of GSH synthesis potentiates temozolomide-induced bystander effect in glioblastoma, Cancer Lett. 1 (2013) 68–75, http://dx.doi.org/10.1016/j.canlet.2012.12.005 (Epub 2012 Dec 12) (PMID:23246370).
[13] J.B. Little, H. Nagasawa, G.C. Li, D.J. Chen, Involvement of the nonhomologous end joining DNA repair pathway in the bystander effect for chromosomal aberrations, Radiat. Res. 159 (2003) 262–267.
[14] R. Baskar, Emerging role of radiation induced bystander effects: cell communications and carcinogenesis, Genome Integr. 1 (2010) 13.
[15] J.S. Dickey, B.J. Baird, C.E. Redon, V. Avdoshina, G. Palchik, J. Wu, A. Kondratyev, W.M. Bonner, O.A. Martin, Susceptibility to bystander DNA damage is influenced by replication and transcriptional activity, Nucleic Acids Res. 40 (2012) 10274–10286.
[16] Y. Ohshima, M. Tsukimoto, H. Harada, S. Kojima, Involvement of connexin43 hemichannel in ATP release after gamma-irradiation, J. Radiat. Res. 53 (2012) 551–557.
[17] L. Aymeric, L. Apetoh, F. Ghiringhelli, A. Tesniere, I. Martins, G. Kroemer, M.J. Smyth, L. Zitvogel, Tumor cell death and ATP release prime dendritic cells and efficient anticancer immunity, Cancer Res. 70 (2010) 855–858.
[18] L. Senovilla, I. Vitale, I. Martins, M. Tailler, C. Pailleret, M. Michaud, L. Galluzzi, S. Adjemian, O. Kepp, M. Niso-Santano, S. Shen, G. Marino, A. Criollo, A. Boileve, B. Job, S. Ladoire, F. Ghiringhelli, A. Sistigu, T. Yamazaki, S. Rello-Varona, C. Locher, V. Poirier-Colame, M. Talbot, A. Valent, F. Berardinelli, A. Antoccia, F. Ciccosanti, G.M. Fimia, M. Piacentini, A. Fueyo, N.L. Messina, M. Li, C.J. Chan, V. Sigl, G. Pourcher, C. Ruckenstuhl, D. Carmona-Gutierrez, V. Lazar, J.M. Penninger, F. Madeo, C. Lopez-Otin, M.J. Smyth, L. Zitvogel, M. Castedo, G. Kroemer, An immunosurveillance mechanism controls cancer cell ploidy, Science 337 (2012) 1678–1684.
[19] M. Bayet-Robert, D. Loiseau, P. Rio, A. Demidem, C. Barthomeuf, G. Stepien, D. Morvan, Quantitative two-dimensional HRMAS ^{1}H-NMR spectroscopy-based metabolite profiling of human cancer cell lines and response to chemotherapy, Magn. Reson. Med. 63 (2010) 1172–1183.
[20] D. Morvan, A. Demidem, Metabolomics by proton nuclear magnetic resonance spectroscopy of the response to chloroethylnitrosourea reveals drug efficacy and tumor adaptive metabolic pathways, Cancer Res. 67 (2007) 2150–2159.
[21] D. Morvan, A. Demidem, S. Guenin, J.C. Madelmont, Methionine-dependence phenotype of tumors: metabolite profiling in a melanoma model using L-[methyl-^{13}C] methionine and high-resolution magic angle spinning ^{1}H–^{13}C nuclear magnetic resonance spectroscopy, Magn. Reson. Med. 55 (2006) 984–996.
[22] C.E. Redon, J.S. Dickey, A.J. Nakamura, I.G. Kareva, D. Naf, S. Nowsheen, T.B. Kryston, W.M. Bonner, A.G. Georgakilas, O.A. Sedelnikova, Tumors induce complex DNA damage in distant proliferative tissues in vivo, Proc. Natl. Acad. Sci. U. S. A. 107 (42) (2010) 17992–17997, http://dx.doi.org/10.1073/pnas (Epub 2010 Sep 20) (PMID:20855610).
[23] T.W. Fan, P. Yuan, A.N. Lane, R.M. Higashi, Y. Wang, A.B. Hamidi, R. Zhou, X. Guitart, G. Chen, H.K. Manji, R. Kaddurah-Daouk, Stable isotope-resolved metabolomic analysis of lithium effects on glial–neuronal metabolism and interactions, Metabolomics 6 (2010) 165–179.
[24] M.A. Selak, S.M. Armour, E.D. MacKenzie, H. Boulahbel, D.G. Watson, K.D. Mansfield, Y. Pan, M.C. Simon, C.B. Thompson, E. Gottlieb, Succinate links TCA cycle dysfunction to oncogenesis by inhibiting HIF-alpha prolyl hydroxylase, Cancer Cell 7 (2005) 77–85.
[25] I. Martins, A. Tesniere, O. Kepp, M. Michaud, F. Schlemmer, L. Senovilla, C. Seror, D. Metivier, J.L. Perfettini, L. Zitvogel, G. Kroemer, Chemotherapy induces ATP release from tumor cells, Cell Cycle 8 (2009) 3723–3728.
[26] L. Zitvogel, O. Kepp, L. Aymeric, Y. Ma, C. Locher, N.F. Delahaye, F. Andre, G. Kroemer, Integration of host-related signatures with cancer cell-derived predictors for the optimal management of anticancer chemotherapy, Cancer Res. 70 (2010) 9538–9543.
[27] A. Ramirez de Molina, D. Gallego-Ortega, J. Sarmentero, M. Banez-Coronel, Y. Martin-Cantalejo, J.C. Lacal, Choline kinase is a novel oncogene that potentiates RhoA-induced carcinogenesis, Cancer Res. 65 (2005) 5647–5653.
[28] J.A. Menendez, R. Lupu, Oncogenic properties of the endogenous fatty acid metabolism: molecular pathology of fatty acid synthase in cancer cells, Curr. Opin. Clin. Nutr. Metab. Care 9 (2006) 346–357.

[29] K.S. Opstad, B.A. Bell, J.R. Griffiths, F.A. Howe, An investigation of human brain tumour lipids by high-resolution magic angle spinning ^{1}H MRS and histological analysis, NMR Biomed. 21 (2008) 677–685.
[30] A. Baracca, F. Chiaradonna, G. Sgarbi, G. Solaini, L. Alberghina, G. Lenaz, Mitochondrial complex I decrease is responsible for bioenergetic dysfunction in K-ras transformed cells, Biochim. Biophys. Acta 1797 (2009) 314–323.
[31] J.C. Wolfman, S.M. Planchon, J. Liao, A. Wolfman, Structural and functional consequences of c-N-Ras constitutively associated with intact mitochondria, Biochim. Biophys. Acta 1763 (2006) 1108–1124.
[32] F. Chiaradonna, D. Gaglio, M. Vanoni, L. Alberghina, Expression of transforming K-Ras oncogene affects mitochondrial function and morphology in mouse fibroblasts, Biochim. Biophys. Acta 1757 (2006) 1338–1356.
[33] S. Nugent, C.E. Mothersill, C. Seymour, B. McClean, F.M. Lyng, J.E. Murphy, Altered mitochondrial function and genome frequency post exposure to γ-radiation and bystander factors, Int. J. Radiat. Biol. 86 (2010) 829–841.
[34] H. Zhou, V.N. Ivanov, Y.C. Lien, M. Davidson, T.K. Hei, Mitochondrial function and nuclear factor-kappaB-mediated signaling in radiation-induced bystander effects, Cancer Res. 68 (2008) 2233–2240.
[35] C. Trainor, K.T. Butterworth, C.K. McGarry, S.J. McMahon, J.M. O'Sullivan, A.R. Hounsell, K.M. Prise, DNA damage responses following exposure to modulated radiation fields, PLoS One 7 (2012) e43326.
[36] K.T. Butterworth, C.K. McGarry, C. Trainor, J.M. O'Sullivan, A.R. Hounsell, K.M. Prise, Out-of-field cell survival following exposure to intensity-modulated radiation fields, Int. J. Radiat. Oncol. Biol. Phys. 79 (2011) 1516–1522.